ELSEVIER

Cement & Concrete Composites 22 (2000) 17–27

Cement & Concrete Composites

Seismic retrofitting of expressway bridges in Japan

Tatsuo Ogata [a,*], Koji Osada [b]

[a] Bridge and Structural Engineering Division, Tokyo Construction Bureau, Japan Highway Public Corporation, 3-39-9, Shiba, Minato-ku, 105-0014, Japan

[b] Bridge Section Expressway Research Institute, Japan Highway Public Corporation, 1-4-1, Tadao, Machida-shi, Tokyo 194-8508, Japan

Abstract

Infrastructures in Japan suffered severe damage in the Hyogoken–Nambu earthquake that occurred on 17 January 1995. The expressway bridges operated by Japan Highway Public Corporation (JH) also had serious damage. According to the lessons from experience of the earthquake, JH has been constructing highway networks having higher seismic reliability as an emergency transporting lifeline, and has been urgently implementing seismic retrofit work. This paper consists of two chapters. First, the outline of seismic retrofit of reinforced concrete piers is described. Second, the seismic retrofit of high hollow circular reinforced concrete piers having cut-off of longitudinal reinforcement and changed wall thickness along the height with carbon fiber sheets is indicated.

Keywords: Reinforced concrete pier; Reinforcement cut-off; Hollow circular cross section; Shears; Seismic strengthening; Carbon fiber sheet

1. Seismic retrofit of expressway bridges

1.1. Basic policy of seismic retrofit

Japan Highway Public Corporation (JH) is in charge of construction and operation of highway and toll road network. The total length of the network operated by JH is about 6500 km. From the experience of Hyogoken–Nambu earthquake that occurred on 17 January 1995, the three-year seismic retrofit projects for expressway bridges have been established throughout Japan, and JH has been implementing seismic retrofit. The retrofit priority is determined under consideration of area, population and situations. Tokai, south of Kanto, Hanshin areas are considered to have high seismic risk. Therefore the bridges in these areas are given higher priority. The bridges in Tomei and Meishin expressway are also given higher priority because of the population they support. The bridges crossing railways or other highways are also given higher priority. JH has already finished retrofitting about 6200 piers with these policies.

1.2. Outline of seismic retrofit design

Superstructures, substructures, foundations, and aseismatic connectors determine seismic behavior of bridges. Therefore it is important for seismic design of bridges to consider seismic structural behavior of the whole system. Retrofit of substructures and implementing bridge-fall prevention devices have to be carried out simultaneously. In the cases of JH project, if vicinity of site permits, these works are carried out at the same time. Replacement or strengthening of bearing is also carried out to support seismic force. If the mass of the superstructure is too heavy to retrofit piers, total structural behavior, for instance natural period must be improved to reduce seismic demand to the piers.

There are two seismic retrofit ways for reinforced concrete piers. The first way is to give piers enough ductility, and the other way is to make piers to have enough strength. Considering the cost of the project and the strength of foundations, the first way is better than the second one. However, if the design seismic force is too large to adopt only the first way due to residual deformation or other reasons, we have to adopt both the ways for retrofit.

If the pier would show shear failure or failure at the cut-off section of longitudinal bars, restoration from seismic damage after earthquakes would be difficult.

* Corresponding author.

0958-9465/00/$ - see front matter
PII: S0958-9465(99)00045-1

Therefore, we have to design piers to fail in flexure at the bottom end.

1.3. Seismic retrofit method

There are three methods for seismic retrofit of reinforced concrete piers. These are reinforced concrete jacketing, steel plate jacketing, and carbon fiber sheets jacketing. The best method is determined among them considering cost, vicinity of construction site, and handling of jacketing materials etc. Reinforced concrete jacketing has the advantage of cost for construction and maintenance compared with the other two methods. So if there is no restriction, reinforced concrete jacketing will be adopted. But in the case of construction site having restriction of clearance, for instance crossing road, railway or river, reinforced concrete jacketing cannot be adopted because this method increases the thickness of pier about 0.5 m comparing with the other two methods which increase only a few centimeters.

The seismic retrofit methods adopted by JH consist of 85% of reinforced concrete jacketing, 7% of steel plate jacketing, and 7% of carbon fiber sheets jacketing.

2. Seismic retrofit of high hollow circular reinforced concrete piers having cut-off of longitudinal reinforcement and varied wall thickness

In expressways where milder horizontal alignment and longitudinal slope are required, high piers exist in sections in mountainous areas. Some of these high piers are higher than 50 m, and are designed to have a hollow cross-section to minimize self-weight. The longitudinal reinforcement is terminated at several levels for reducing costs.

Since seismic retrofit of high piers has been conducted in few cases and has many restrictions, a number of engineering decisions have to be made for planning and designing of seismic retrofit.

Hereafter, the planning, tests and design of seismic retrofit of hollow circular piers with an average height of 53 m are reported.

2.1. Seismic retrofit planning

Outline of piers for retrofit: Fig. 1 shows the area around the retrofit work site. The piers are of a circular cross-section with the height ranging from 42 to 65 m, and are located near the boundary between Kanagawa and Shizuoka Prefecture on the Tomei Expressway. They stand on the Sakawa River (Figs. 2 and 3).

In these piers, longitudinal bars are cut-off at four vertical midpoints. The cross-section is hollow with the thickness gradually decreasing upward from the solid bottom to 2, 1.5, 1 and 0.6 m.

Fig. 1. Construction site and vicinity.

Fig. 2. Location of construction site.

Planning of seismic retrofit: Fig. 4 shows a planning procedure for seismic retrofit. Verification of seismic performance of existing piers revealed that failure in cut-off sections would proceed before the failure at the bottom of the pier. Retrofit of the existing piers was, therefore, considered necessary for the cut-off sections. Work was then started to identify the restrictions and implementation conditions on the site.

Since the piers stand on the river and their blocking ratio had to be considered, reinforced concrete jacketing could not be adopted because it would involve an increase of the cross-section of the pier. Due to water withdrawal from upstream dams during the flood season, operation of heavy and large equipment in the river is impossible. During the flood season, therefore, use of lifts was considered necessary. Retrofit materials would have to be either transported manually from outside the river or lifted into the river using a large-scale temporary

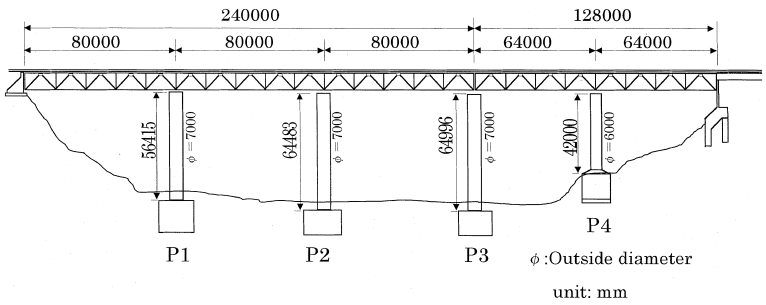

Fig. 3. General drawing of piers.

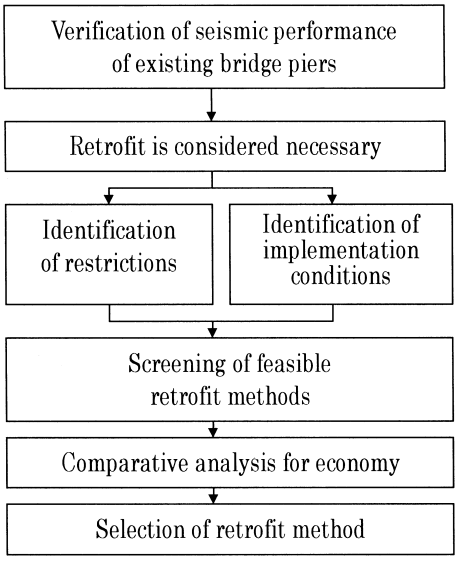

Fig. 4. Procedure for seismic retrofit planning.

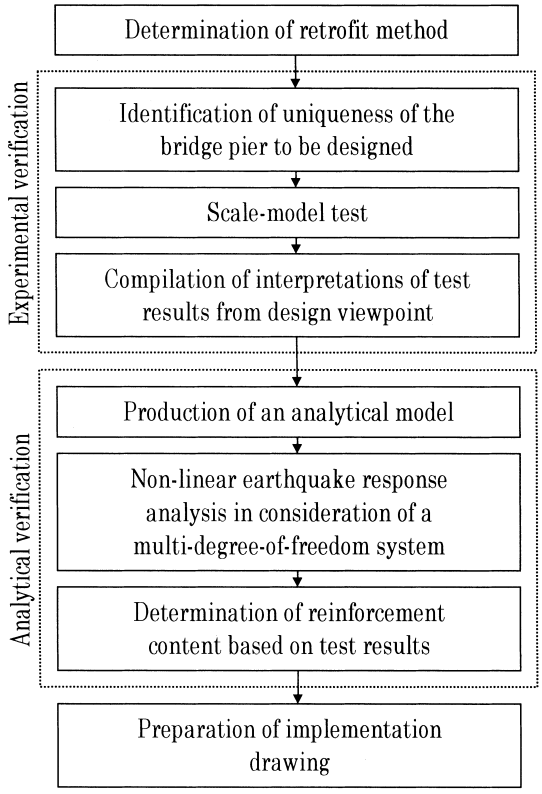

Fig. 5. Experimental and analytical verification of CFS jacketing.

structure. According to those considerations, steel jacketing which would involve the transportation of heavy materials or erection of a temporary structure was rated unfavorably. Finally, the carbon fiber sheet (CFS) jacketing was adopted.

The pier is hollow and circular, and has cut-off sections at several levels. In addition the top level has a very thin concrete cross-section. Therefore, the tests [1,2] described later were conducted with a scale model to reflect the results in seismic retrofit design.

Fig. 5 shows the verification of CFS jacketing.

2.2. Scale-model test

Shape of the specimen: Since the study was focused on the hollow structure, the specimen was created as close as possible to the actual structure as a one-20th scale model without the solid portion to reflect mechanical properties of the actual structure. The shape and dimensions of the specimen are shown in Fig. 6 and Table 1, respectively. The specimen was fabricated as an out-

standing single column with a footing. Up to the 1600-mm height from the top of the footing, longitudinal bars were cut-off at three different levels, and the cross-sections were hollow with varied thicknesses. The upper part of the column, where the axial and lateral loads were applied, had a square section. For convenience of subsequent discussion, the pier is divided into four zones, I through IV from the bottom, with cut-off points regarded as boundaries. The cross-section at the top of the footing is represented as Ir, and other three sections at cut-off points are represented as Ic, IIc and IIIc, respectively. A total of five specimens were fabricated. The number of specimens without any additional reinforcement (hereinafter referred to as non-reinforced

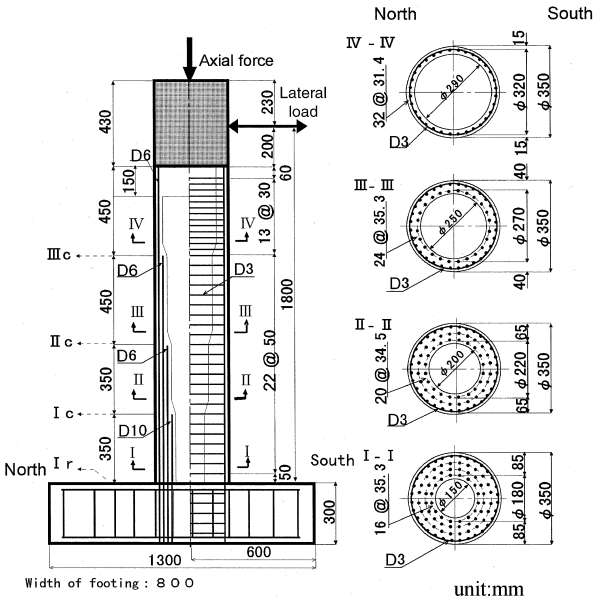

Fig. 6. Shape of specimen.

specimens) is two, and three for the specimens reinforced with CFS.

Mechanical properties of the concrete and reinforcement used in the column specimens are shown in Tables 2 and 3, respectively. The maximum size of coarse aggregate in concrete was set at 10 mm. Table 4 shows the mechanical properties of CFS which were attached to specimens.

In the tests, an axial compressive force of 73.5 kN was applied to all the specimens. The minimum stress applied was 0.94 MPa in zone I, and the maximum stress was 2.44 MPa in zone IV.

Characteristics of reinforced specimens: The area and the weight of CFS for each reinforced specimen are shown in Fig. 7.

For specimen PS–CF–ST, CFS were applied mainly in the longitudinal direction to mitigate drastic variations in the content of longitudinal bars at cut-off points, and to confirm that the ultimate failure would take the form of flexural failure at the foot of the column. The CFS volume required was determined by representing CFS as reinforcement through multiplication of CFS cross-section, and ratios of tensile strength and modulus of elasticity to those for ordinary steel reinforcement. As a result, the volume was set at 200 g/m^2 for cross-section 4, and at 150 g/m^2 each for cross-sections IIc and IIIc. CFS in the hoop direction were aimed at enabling smooth transfer of stress of longitudinal CFS and thus were in relatively small quantities. Strips of about 6000 carbon fibers were radially bonded with a 40-mm-pitch. Fiber area weight was 10 g/m^2, one-fifth of the weights of other specimens. The weight and area of CFS for

Table 1
Dimensions of specimen

Specimen[a]	Longitudinal (%)				Carbon fiber in the longitudinal direction (area ratio in %)[b]				Hoop (%)				Carbon fiber in the hoop direction (area ratio in %)[b]				Axial compressive force (kN)	Loading method
	Zone I	Zone II	Zone III	Zone IV	Zone I	Zone II	Zone III	Zone IV	Zone I	Zone II	Zone III	Zone IV	Zone I	Zone II	Zone III	Zone IV		
PS–N–ST																		
PS–NC–ST	32-D6	32-D6	32-D6	32-D6														
PS–CF–ST	24-D6	24-D6	24-D6	(3.4)	–	Four layers (0.199)	Three layers (0.19)	–	D3@50 (0.14)	D3@50 (0.19)	D3@50 (0.28)	D3@50 (0.78)	–	One layer (7.4×10^{-3})	One layer (1.1×10^{-2})		73.5	Static
	20-D6	20-D6	(3.8)															
PS–CF2–ST	16-D10	(3.7)			–	Two layers (0.09)	Two layers (0.13)	–										
PS–CF3–ST	(4.5)				–	–	–	–						One layer (3.7×10^{-2})	One layer (5.6×10^{-2})	One layer (9.3×10^{-2})		–

[a] (PS: Series name)–(N: Non-reinforced/NC: Non-reinforced, with compressive strength of column concrete 1.8 times that for N/CF, CF2 and CF3; Reinforced with carbon fibres)–(ST: Static test).
[b] Values obtained by calculation as for reinforcement, on the assumption of uniform application of carbon fibers with design thickness.

Table 2
Mechanical properties of concrete

Specimen	Compressive strength (MPa)	Tensile strength (MPa)	Young's modulus (GPa)	Compressive strength of soild concrete (MPa)
Specimen other than PS–NC–ST	27[a]	2.3[a]	18[a]	33[b]
PS–NC–ST	45	2.8	21	23

[a] Average value.
[b] Average value.

Table 3
Mechanical properties of reinforcing bars

Type		Yield strength (MPa)	Tensile strength (MPa)	Young's modulus (GPa)[a]	Applied to
Size	Standard				
D3		319	412	191	Hoop
D6	SD345	401	502	178	Longitudinal bar
D10	SD295A	340	495	175	Longitudinal bar

[a] Obtained using distortion value measured by a distortion gauge attached to reinforcement, and nominal cross section.

Table 4
Mechanical properties of CFS

Fiber area weight (g/m^2)	Design thickness (mm)[a]	Tensile strength (MPa)[b]	Young's modulus (GPa)[b]
50	0.028	4167	231

[a] Fiber cross section is divided by the width, and multiplied by a ratio between the width and pitch.
[b] Results of test using 12.5 mm wide, 0.28 mm thick test pieces made by impregnation of resin.

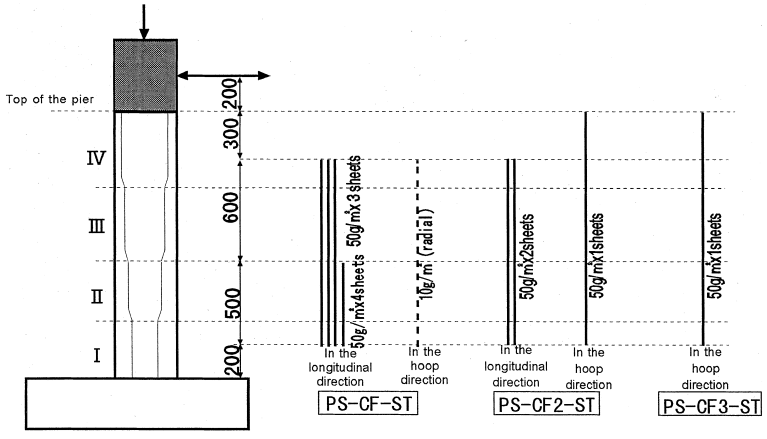

Fig. 7. Weight and area of reinforcing carbon fiber sheet.

specimens PS–CF2–ST and PS–CF3–ST, were determined in view of the test results for PS–CF–ST. CFS in the longitudinal direction were decreased while those in the hoop direction increased. PS–CF3–ST, in particular, was reinforced with CFS in the hoop direction only.

Loading method: Two actuators were used for loading. As shown in Fig. 6, a lateral force or lateral displacement was applied while placing a certain axial force on the top of the column. The same loading method was adopted for five specimens. The positive/negative average of lateral displacements at loading point, when the yield load calculated in cross-section Ir of specimen PS–N–ST was 59.4 kN, was assumed to be δy. Alternating positive and negative loads were basically applied only once for each stage of displacement, based on the results of various past pseudo-dynamic loading tests [3], until

the end of loading while increasing the displacement by 1 δy. Loads were applied laterally to the pier axis in the north-south direction as shown in Fig. 6. Cracks were measured on the west side.

2.3. Test results and comments

Load-bearing behavior and ductility ratio: Envelopes of load-displacement curves obtained by the loading tests for specimens PS–N–ST and PS–NC–ST are shown in Fig. 8.

Results of the tests are listed in Table 5. For specimen PS–N–ST, yield displacement (δy) was 21.0 mm. At the point, yield strain was already exceeded for the outermost longitudinal reinforcement in cross-sections Ir and Ic. Since the cross-section was circular, the difference between the load causing the outermost longitudinal reinforcement to yield and the ultimate strength was large. With increase in the applied displacement, strength increased, and yielding occurred consecutively upward from the cross-section IIc to IIIc and so on. At the time of displacement of 1.5 δy, the outermost reinforcement at all cut-off points yielded. While the calculated ultimate strength in the cross-section Ir was 87.2 kN, strength decreased from the peak of 74.5 kN at 2 δy due to the extension growth of diagonal cracks between zones III and IV, and at around 3.5 δy suddenly decreased due to the crushing of concrete at the top of the reinforced concrete column. Yield load for PS–NC–ST, with concrete compressive strength 1.8 times that of PS–N–ST, was calculated as 62.8 kN. On PS–NC–ST, the outermost longitudinal reinforcement already yielded in the cross-sections Ir and Ic at 59.4 kN as for PS–N–ST, and at the time of displacement 1.5 times that at the yield point or at a displacement of 8.8 mm (δy), the outermost longitudinal reinforcement at the cut-off points in the cross-sections IIc and IIIc also yielded. Large concrete strength and solid cross-section at the top of the reinforced concrete column resulted in no substantial decrease in strength until +3 δy. The maximum strength was 80.4 kN, slightly larger than that of PS–N–ST. Beyond that point, no concrete crushed at the top of the column unlike PS–N–ST. Load carrying capacity, however, decreased due to shear failure in zones III and IV.

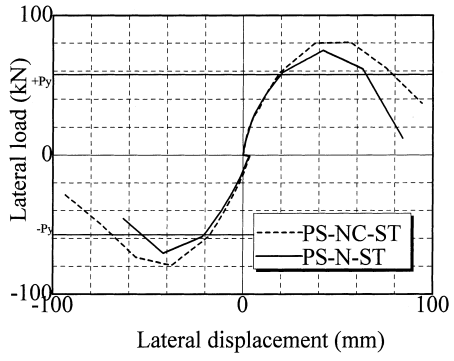

Fig. 8. Envelope of load–displacement curve (1).

Fig. 9 shows the envelopes of the load-displacement curves of the specimens reinforced with CFS, together with that of non-reinforced PS–NC–ST for comparison. As for PS–CF–ST, reinforced mainly longitudinally, flexural failure occurred near the bottom end of CFS reinforcement in cross-section I when $\pm 3\delta y$ was applied. The maximum strength was nearly identical to calculated ultimate strength in cross-section Ir. When $\pm 4\delta y$ was loaded, however, CFS in the hoop direction ruptured at overall height on the east and west sides, and lateral load declined markedly. Final failure mode was shear failure, and the envelope showed a similar shape to that for PS–NC–ST, representing brittle behavior.

For specimen PS–CF2–ST with longitudinal reinforcement content 1/2–1/3 of that for PS–CF–ST, and with reinforcement in the hoop direction five times as large, flexural failure occurred, in which longitudinal reinforcement buckled at the bottom end of CFS reinforcement in zone I, and the strength decreased. No shear failure was observed and ductile behavior was found. CFS reinforcement in the hoop direction was sufficient against shear, but not enough to increase ductility as obvious from existing studies [3]. CFS in the hoop direction finally fractured at the point where longitudinal bars buckled. In the cases of specimens PS–CF–ST and PS–CF2–ST, which were reinforced in the longitudinal direction, the outermost longitudinal bars yielded at all of the cut-off points before the displacement of 1.5 δy as strength exceeded the yield load by 20–30%. No damage to CFS, however, was confirmed at cut-off points.

Specimen PS–CF3–ST, which was reinforced only in the hoop direction, suffered no serious damage such as shear failure and buckling of longitudinal bars even at the time of ultimate loading of ± 5 δy, and displayed ductile behavior without any decrease of lateral load. It was noticeable that reinforcement at cut-off points only in the hoop direction caused the cut-off points to be deformed more easily and resulted in better load-bearing behavior.

The width of cracks due to bending at cut-off points was large, and some of the cracks were left open at the end of loading. The maximum strength was slightly lower than that of those specimens which experienced plastic deformation at the bottom of the column.

Ductility ratio is defined as the ratio of the ultimate displacement to the yield displacement, in which the former was assumed as the displacement at which the applied load reduced the yield one. The ductility ratios for non-reinforced specimens PS–N–ST and PS–NC–ST

Table 5
Results of static alternating repeated loading tests

Specimen	Yield displacement (mm)[a]	Maximum strength (kN[b])	Final loading	Residual strength (kN)[b,c]	Ductility factor	Remarks
PS–N–ST	21.0 (δy_1)	+74.5 (when +2 δy_1 is applied) −70.6 (when −2 δy_1 is applied)	+4 δy_1 −3 δy_1	+12.7 (17%) −46.1 (65%)	2	• Concrete cover in zone IIIc on the east and west sides fell during application of load −3 δy_1. • Concrete at the top of the column on the south side crushed during application of +4 δy_1, and strength deteriorated rapidly.
PS–NC–ST	18.8 (δy_2)	+80.4 (when +3 δy_2 is applied) −79.4 (when −2 δy_2 is applied)	−5 δy_2	+37.2 (46%) −28.4 (36%)	3	• Concrete fell in zones III and IV on the east and west sides about the time when −3.5 δy_2 was applied.
PS–CF–ST	18.1 (δy_3)	+85.3 (when +3 δy_3 is applied) −81.3 (when −3 δy_3 is applied)	−5 δy_3	+45.1 (53%) −39.2 (48%)	3	• CFS in the hoop direction at the bottom end of reinforced column on the south side fractured during application of +3.5 δy_3. • CFS in the hoop direction on the east and south sides fractured for the overall height during application of +4 δy_3.
PS–CF2–ST	19.4 (δy_4)	+84.3 (when +3 δy_4 is applied) −84.3 (when −3 δy_4 is applied)	−5 δy_4	+78.4 (93%) −67.6 (80%)	5 or higher	• CFS in the hoop direction at the bottom end of reinforced column on the southwest side fractured during application of +5 δy_4, and CFS are turned up from the bottom end of reinforced column to cross section Ic. • Longitudinal reinforcement on the compression (south) side buckled, and strength decreased during application of −5 δy_4, and CFS at the bottom end of reinforced column on the north side fractured.
PS–CF3–ST	19.0 (δy_5)	+81.3 (when +2 δy_5 is applied) −81.3 (when −2 δy_5 is applied)	−5 δy_5	+77.4 (95%) −77.4 (95%)	5 or higher	• No buckling of reinforcement occurred until the end of loading, and no strength decrease was observed. • Widths of cracks due to bending at cut off points increased, and concrete at cut off points on the north and south sides slightly delaminated due to crush.

[a] Average of negative and positive values.
[b] Upper values are positive maximum strengths, and lower values indicate negative maximum strengths.
[c] Positive and negative values under final load. Figures in parentheses indicate ratios to maximum strength.

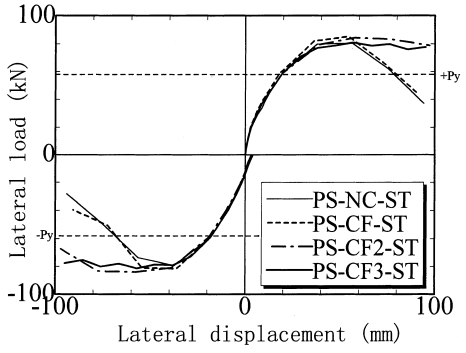

Fig. 9. Envelope of load–displacement curve (2).

are 2 and 3, respectively. The ratio is 3 for PS–CF–ST, which was reinforced mainly in the longitudinal direction. The ratios for PS–CF2–ST and PS–CF3–ST, which had more reinforcement in the hoop direction, are 5 or larger.

Characteristics of damage: Fig. 10(a) and (b) show the conditions of specimen PS–N–ST at −3 δy and of PS–NC–ST at −3.5 δy, respectively. At these points, displacements at the loading point were the same for the two specimens. Damage of these specimens was similar to each other. The damage due to shear failure in zones III and IV, above and below cross-section IIIc, one of

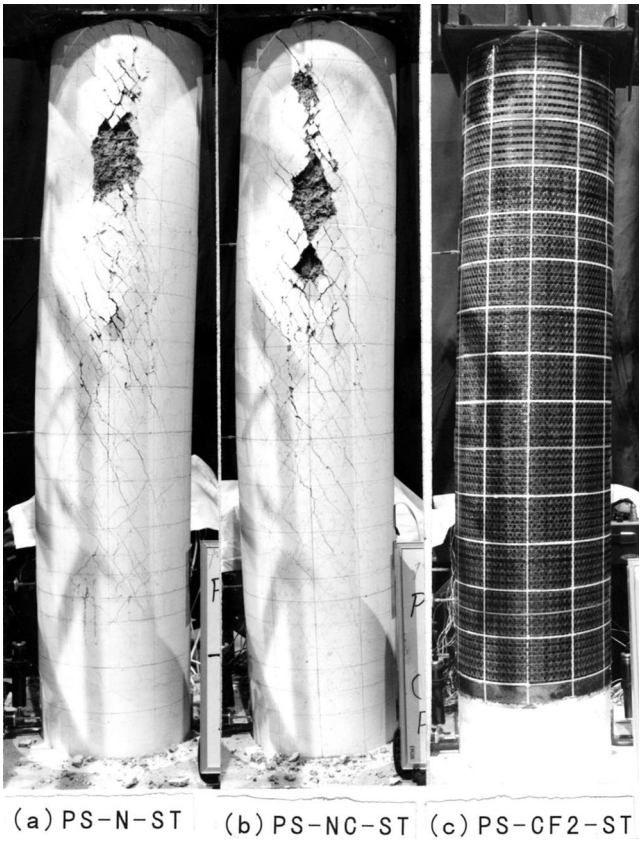

Fig. 10. Cracking conditions (at −3 to 4 δy).

the cut-off points, was severest. Spalling of concrete cover was also observed.

In zone IV, the calculated shear strength was almost the same as the value in zone II and smaller than that in zone III. The ultimate damage, however, was severest in zone IV probably for the reasons related to the percentages of shear force shared by hoops and concrete. The calculated shear strength in zone IV was provided mostly by hoops. When the column is hollow and circular, and has a thin wall, diagonal cracks substantially reduce concrete stiffness, which then reduces axial stiffness of hoops because of curvature of hoops. Diagonal cracks easily grow and concrete is severely damaged. Such a unique form of shear failure was observed in zone IV.

Fig. 10(c) shows the state of reinforced specimen PS–CF2–ST at −4 δy. Displacement was slightly larger than that for non-reinforced specimens. No damage was observed, and the effect of CFS on the maintenance of soundness of the pier was confirmed.

Shape of deformation: Fig. 11 shows the lateral deformations for PS–NC–ST at the cut-off points at different stages of displacement. The lines in the figure suddenly started inclining for displacement on cross-section IIc at around the point where displacement exceeded ±2 δy. This is also the stage of displacement

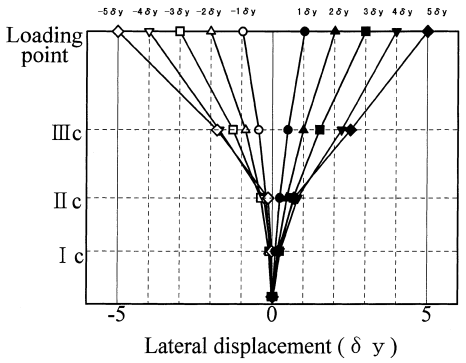

Fig. 11. Deformation conditions (PS–NC–ST).

where shear failure developed in zones III and IV. It is, therefore, assumed that shear deformation increased in zones III and IV. Fig. 12 compares the deformations at ±4 δy between non-reinforced specimen PS–NC-ST and PS–CF–ST which was reinforced with CFS mainly in the longitudinal direction. The figure explicitly shows that whether the specimen is reinforced or not has a considerable influence on the deformation near the bottom of the column and in cross-section IIc.

Ultimate conditions: Fig. 13(a)–(d) show the comparison of the conditions among four specimens at −5 δy or under the ultimate load except for specimen PS–N–ST. The ultimate mode of failure was shear failure in zones III and IV for specimen PS–NC–ST, overall shear failure following buckling of longitudinal bars at the bottom end of CFS-reinforced portion for PS–CF–ST, flexural failure accompanied by buckling of longitudinal bars at the bottom end of CFS-reinforced portion for PS–CF2–ST, and flexural failure at cut-off points for PS–CF3–ST. A review of the effect of CFS on the reinforcement of cut-off points, based on the ultimate condition, shows that reinforcement in the longitudinal direction controlled the growth either of flexural or diagonal cracks at cut-off points, thus mechanical properties of cut-off points were improved, and that the failure point moved to the bottom of the column. In the case where the column was reinforced with CFS in

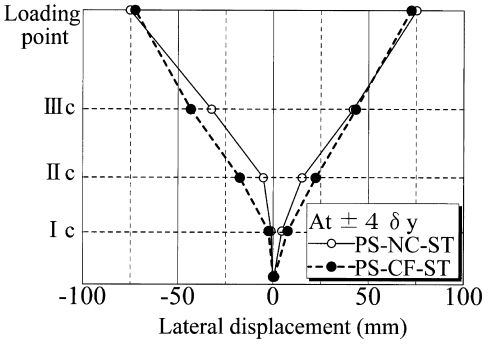

Fig. 12. Comparison of deformation conditions.

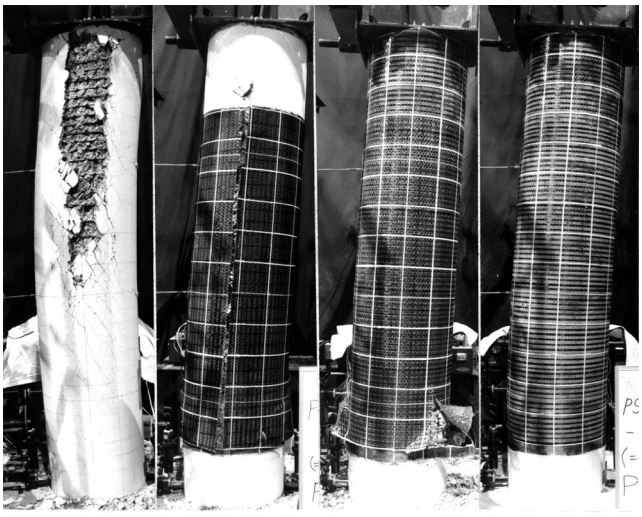

Fig. 13. Conditions at $-5\ \delta y$.

the hoop direction, on the other hand, it is shown that no growth of flexural cracks could be controlled from cut-off points, but the growth of diagonal cracks could be prevented. Improvement of mechanical properties at the cut-off points was also confirmed by Fig. 12 and by the deformation condition shown in Fig 13. It was noticed that there appeared an vertical straight slip of CFS in specimen PS–CF–ST at all over the shear surface. This is because few CFS in the hoop direction caused failure in the ultimate state, and caused vertical CFS to slip.

Fig. 14(a)–(c) show the conditions of specimens after CFS were peeled off. Fig. 14(a) shows the condition of specimen PS–CF–ST on the surface in loading direction (the west surface). It is clear that the surface of concrete delaminated all over with a uniform width, and that the concrete on the surface transverse to the loading direction (north-south surface) at the bottom end of reinforcement crushed. Fig. 14(b) and (c) show zones I and II on the north side of specimens PS–CF2–ST and PS–CF3–ST, respectively. For specimen PS–CF2–ST, concrete at the bottom end of reinforced portion was destroyed, and longitudinal bars buckled. No noticeable damage was, however, observed in any other area. Only traces of flexural and diagonal cracks remained in non-reinforced areas in zone IV. In specimen PS–CF3–ST, no serious damage was observed but remaining flexural cracks were observed overall, and traces of diagonal cracks, although in small numbers, were also found. There was also delamination of concrete cover due to local crush near cross-section Ic. Specimen PS–CF2–ST seems to have suffered greater damage than PS–CF3–ST, but damaged locations were limited and ultimate strength was slightly larger.

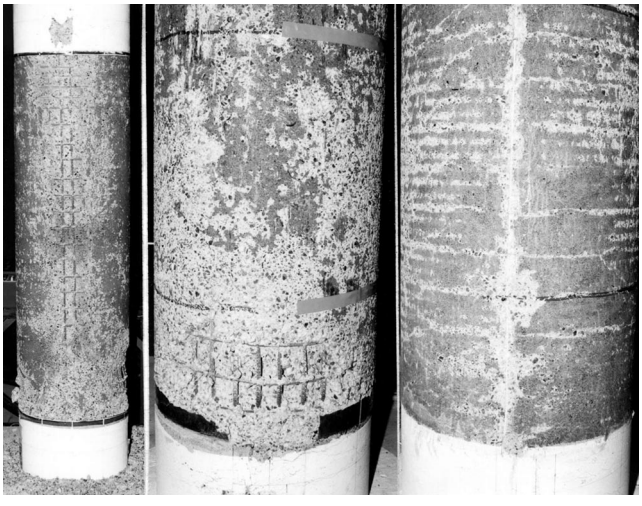

Fig. 14. Conditions after CFS were peeled off.

2.4. Experimental results for seismic retrofit design

As a result of loading tests for studying mechanical properties and seismic retrofit of reinforced concrete piers with varying longitudinal reinforcement contents and wall thicknesses under large seismic forces, the following conclusions were reached.

(1) It was revealed that hollow circular reinforced concrete column specimens might show shear failure in a brittle manner under a seismic force much larger than the design force.

(2) The CFS content in the longitudinal direction, required to control the curvature arising from cut-off of reinforcement and to shift to flexural failure at the bottom of the column, was calculated in terms of reinforcement content by multiplication of CFS cross-section, and ratios of tensile strength and modulus of elasticity to those for ordinary reinforcement, and proved sufficient. In addition, even with a decrease of longitudinal CFS content, shear failure due to cut-off of reinforcement could be prevented if sufficient reinforcement against shear was applied. Therefore, no strength deterioration at the time of large deformation was observed and ductile load-bearing behavior was recognized. When the longitudinal CFS content was none, an increase in the width of flexural cracks at cut-off points became remarkable.

(3) A unique mode of shear failure was displayed when the specimen was hollow and circular, and had a thin wall. Diagonal cracks substantially reduced concrete stiffness, which then reduced axial stiffness of hoops because of curvature of hoops. Diagonal cracks easily grew and concrete was severely damaged.

(4) CFS with a fiber area of 50 g/m^2 was found sufficient for the shape and dimension of the specimen for

controlling shear failure unique to a hollow circular concrete with a thin wall.

In the experiment, influences of vertical distribution of column weight could not be re-created because of the restriction on loading method. Non-linear earthquake response analysis in consideration of a multi-degree-of-freedom system was conducted with a fiber model, using the seismic wave form suggested in the Standard Specifications for Highway Bridges.

Fig. 15 shows a conceptual view of the fiber model used in the analysis and the maximum response accelerations obtained for a standard pier as a result of non-linear earthquake response analysis in consideration of a multi-degree-of-freedom system.

As a result of the analysis, it was found that type-I seismic wave (inter-plate type) had larger response acceleration because the pier had a long natural period. The maximum response acceleration was largest at the center of gravity of the superstructure at around 600 gal, and tended to decrease downward. The first mode was predominant. The tendency of response acceleration to decrease was declining at the middle height, and a slight influence of the second mode of vibration was also observed. Fig. 16 is a comparison between bending moment acting during an earthquake and the bending strength of the existing pier before retrofit. As shown in the figure, it was revealed that the design response acceleration caused no yielding around the bottom, but the yield point had already been reached in cut-off sections. Reinforcement was, therefore, applied to prevent the cut-off sections from yielding until the yield around the bottom. The acting bending moment at the time of yield around the bottom was obtained based on the assumption that maximum response acceleration increased at the same rate at all heights until yielding of the bottom.

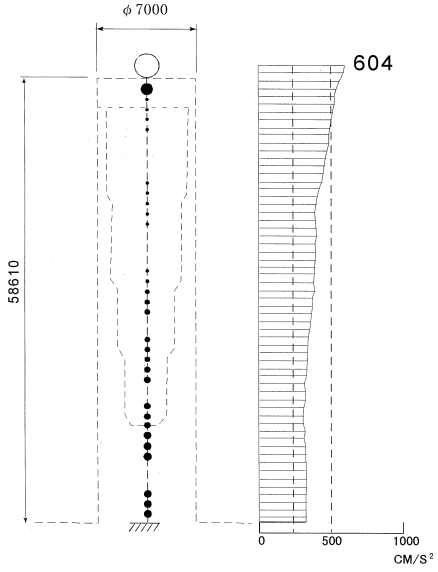

Fig. 15. Analytical model and maximum response accelerations.

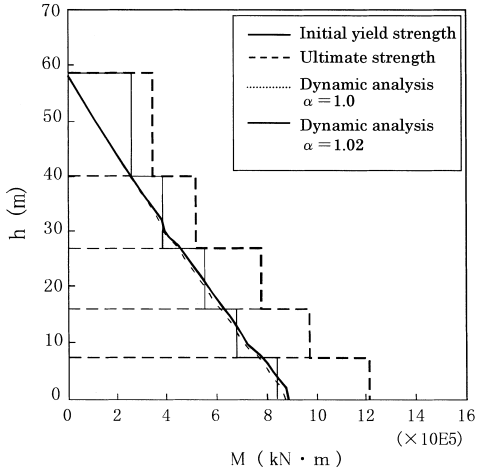

Fig. 16. Comparsion between seismic bending moment and bending strength.

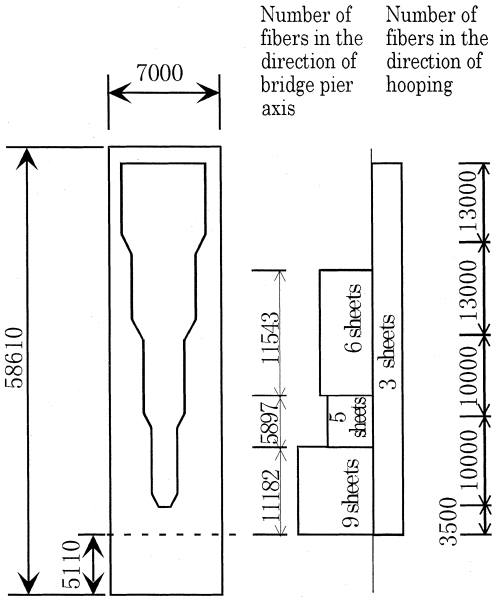

Fig. 17. Content of carbon fibers.

The content of carbon fiber sheets, attached to compensate for the lack of strength against the bending moment obtained above, was calculated at about two to nine layers of 300 g/m^2 carbon fiber sheets by regarding carbon fiber sheets as reinforcing bars. Fig. 17 shows the contents of carbon fibers for a typical pier.

3. Closing remark

As a result of loading tests to verify the seismic performance of high hollow circular piers retrofitted by

Fig. 18. Application of CFS jacketing.

CFS jacketing, the effect of the CFS jacketing on the prevention of shear failure was verified. The CFS content was determined by a non-linear earthquake response analysis in consideration of a multi-degree-of-freedom system. Figs. 18 and 19 show the application of the CFS jacketing.

This retrofit work was carried out [4] by the Tokyo 1st Operation Bureau of the Japan Highway Public

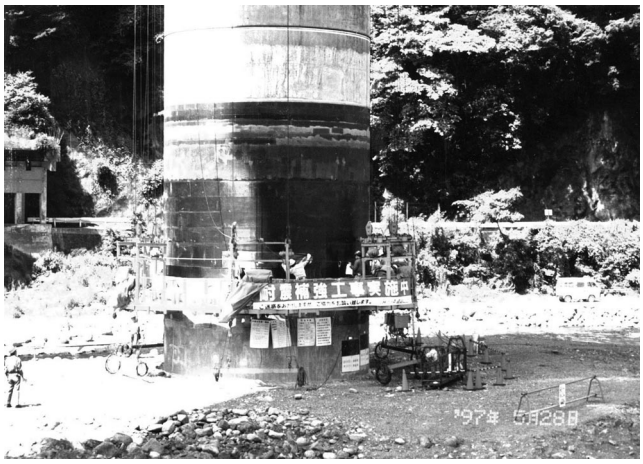

Fig. 19. Application of CFS jacketing.

Corporation, and completed in March 1998 without any trouble. The authors would like to pay tribute to the individuals who made contribution to the work.

References

[1] Osada K, Okawa S, Nishi, K, Ikeda S. Retrofit of hollow circular concrete bridge piers with carbon fiber sheets (in Japanese). Proceedings of the 52nd annual lecture meeting of the Japan Society of Civil Engineers, Part 5, September 1997, pp. 622–3.

[2] Osada K, Yamaguchi T, Ikeda S. Seismic performance and strengthening of hollow circular RC piers having reinforcement cut-off planes and variable wall thickness (in Japanese). Proceedings of the Japan Concrete Institute 1999;10(1):13–24.

[3] Osada K, Ohno S, Yamaguchi T, Ikeda N. Seismic performance of reinforced concrete piers reinforced with carbon fiber sheets (in Japanese). Proceedings of the Japan Concrete Institute 1997:8(1):189–203.

[4] Osada K, Nagashima A, Terada K, Nishi K. Planning and design of retrofit of hollow circular piers with reinforcement-cut-off at multiple stages (in Japanese). Proceedings of the 53rd annual lecture meeting of the Japan Society of Civil Engineers, October 1998.